Radar Systems and
Remote Sensing Laboratory

RADAR BACKSCATTER MEASUREMENTS FROM SIMULATED SEA ICE:

CRRELEX'93 RESULTS

THE UNIVERSITY OF KANSAS CENTER FOR RESEARCH, INC.
2291 Irving Hill Road
Lawrence, Kansas 66045-2969

(11)

RADAR BACKSCATTER MEASUREMENTS FROM SIMULATED SEA ICE:

CRRELEX'93 RESULTS

P. Kanagaratnam, S. P. Gogineni and S. Beaven

Radar Systems and Remote Sensing Laboratory
Department of Electrical Engineering and Computer Science, University of Kansas
2291 Irving Hill Road, Lawrence, Kansas 66045-2969
TEL: 913/864-4835 * FAX: 913/864-7789 * OMNET: KANSAS.U.RSL

K. C. Jezek and I. Zabel

Byrd Polar Research Center, The Ohio State University
108 Scott Hall, 1090 Carmack Road, Columbuc OH 43210-1002
TEL: 614/292-7973 * FAX: 614/292-4697 * OMNET: KJEZEK

RSL Technical Report 8243-3

June 1994

Sponsored by:

Office of Naval Research, Arlington VA 22217-5000
Grant N00014-89-J-1456

1. Introduction

We performed radar backscatter measurements on artificially grown sea ice in an indoor facility at the US. Army Cold Regions Research and Engineering Laboratory (CRREL) during the 1993 winter season. The objectives of these experiments were to study various mechanisms for simulating roughness and to better understand backscatter mechanisms.

These backscatter measurements were made at 13.9 GHz and for incident angles ranging from 0° to 55° with all four linear polarization combinations: VV, HH, VH & HV. In addition to the backscatter measurements from saline ice, the return from three calibration targets were measured. These targets included a Luneburg lens, a metal sphere and a dihedral corner reflector. These measurements were made to enable us to remove the systematic errors due to polarization impurity of the antenna and other system effects.

2. CRRELEX'93 Experiment Description

We used three techniques to simulate sea ice surfaces with varying roughness. They are

1) Adding a thin snow layer and allowing it to adhere to the ice surface,

2) Adding a layer of chipped ice to the ice surface, and

3) Spraying water on the layer of chipped ice to make them adhere to the ice surface.

Unusually warm weather did not allow for the timely growth of ice at the outdoor facility in 1993. This has since been corrected by the construction of CRREL's new refrigeration unit at the outdoor Geophysical Research Facility. Since the weather did not permit outdoor measurements, the experiment utilized the indoor pit facility at CRREL where sea ice was simulated with varying roughness. This facility provides a test bed for experimentation under quasi-laboratory conditions. The experiment was carried out from January 8th to January 16th. During this period, backscatter measurements were taken from bare ice with increasing thickness. On Jan. 14 measurements were made using the first roughening technique with a thin snow layer on bare ice. On Jan. 15 measurements were made using the second roughening technique with chipped ice added to ice surface. On Jan. 16 measurements were made on slushy ice. The slushy ice condition was simulated by drilling holes in the ice, thus allowing water below the ice surface to flow out of these

holes and into the snow/ice interface. This simulates the negative freeboard condition often found in the sea ice surrounding Antartica. Table 1.1 gives a summary of the data set.

Table 2.1 CRRELEX'93 Data Summary

Date	Time	Angles	Number of Spots	Thickness (mm)	Temp. (°C)	
					Room	Ice Surface
8 Jan	11:35pm	0°-55°	4	2	-16.3	-12.8
9 Jan	2:15pm	0°-55°	4	35	-19	-16.7
10 Jan	10:40am	0°-55°	4	75	-17.8	-15.7
10 Jan	2:40pm	0°-55°	4	90	-17.8	-15.7
11 Jan	1:28pm	0°-55°	4	110	-17.9	-16.5
12 Jan	10:40am	0°-55°	4	158	-19.1	-17.6
13 Jan	9:45am	0°-55°	2	160		
14 Jan	4:15pm	0°-55°	4	240mm. with snow on top.		
15 Jan	9:50am	0°-55°	2	Ice cubes		
16 Jan	3:25pm	0°-55°	4	Slushy ice		

3. Step-Frequency Radar System

3.1 *Description*

The measurements were made at Ku band with a network-analyzer-based step frequency system. The system contains an HP 8753C Network Analyzer as the core.

The RF sections provided the up-conversion of the network analyzer output from 2 GHz center frequency (IF) to a center frequency of 13.9 GHz. The network analyzer generated was used to coherently measure the amplitude and the phase of the returned signal at IF, for a set of discrete frequencies. The frequency of the network analyzer was stepped through 1000 MHz of bandwidth in 2.5 MHz steps resulting in 15-cm range resolution.

The switching network in the RF section guides the signal to either the horizontal or vertical polarization port of the antennas. This allows the transmission of both vertical and horizontal polarization. The backscattered signal is collected with the receive antenna and is separated into vertical or horizontal polarization by the switching network. The returned signal is then mixed down to IF for measurement with the network analyzer. Table 3.1 gives the specifications of the system used.

Table 3.1 Specification of Ku-band radar

Center Frequency. (GHz)	13.9
RF Bandwidth (MHz)	1000
Free-space Resolution (cm)	15
Number of frequency steps	400
Footprint in cm (2m range)	30 x 30
Transmit power (mW)	10

3.2 *Principles*

The step frequency radar was used to measure the scattering coefficients (σ°) of saline ice. The radar was calibrated using the complex vector calibration technique.

To determine the backscattering coefficients we have to first obtain the voltage scattering coefficient from the target. The voltage scattering coefficient s_k of the target is related to the IFFT of the data by (Izuka et al., 1984),

$$h_k = \frac{N s_k E_o}{z_k^2} e^{j\left(\frac{4\pi}{c}\right)(kf_o \Delta z)},$$

where h_k is the complex spectral component of the measured data at point k,

N is the total number of samples over the bandwidth,

E_o is the incident electric field magnitude,

z_k is the distance from the radar to the scattering point in question,

c is the velocity of light,

f_o is the lowest operating frequency, and

Δz is the resolution.

The power returned is simply the square of the magnitude of the voltage scattering coefficient.

4. Complex Vector Calibration Technique

The complex vector calibration technique is used to reduce errors in radar measurements due to the frequency response of RF components in the radar system and polarization impurity. Polarization impurity can cause significant errors in cross polarized measurements. The calibration

required the use of three calibration targets; a sphere, a diplane in two orientations and a Luneburg lens. The details of the calibration technique can be found in (Beaven, 1992). The corrected return power is then used to compute σ° with narrow beam approximation to the radar equation as

$$\sigma^{\circ} = \frac{P_r \sigma_{cal} R^4 P_{dlcal}}{P_{cal} R_{cal}^4 A P_{dl}},$$

where P_r is the vector corrected power return from the target,

P_{cal} is the vector corrected power return from a calibration target of known radar cross section,

σ_{cal} is the radar cross section of the calibration target,

P_{dl} is the delay line reading taken at the time of field measurement,

P_{dlcal} is the delay line reading taken at the time of calibration,

R is the range to the target,

R_{cal} is the range to the calibration target, and

A is the area illuminated by the antenna.

The illuminated area is computed as,

$$A = \frac{\pi}{2} \frac{R_0^2}{\cos(\theta)} \tan\left(\frac{\beta}{2}\right) \left[\tan\left(\theta + \frac{\beta}{2}\right) - \tan\left(\theta - \frac{\beta}{2}\right) \right],$$

where ß is the antenna beamwidth,

θ is the incidence angle, and

R_0 is the 0° range to the target.

The vector calibration resulted in a 10 -20 dB reduction in the cross-polarized measurements. The plots of the backscattering coefficients with and without vector correction are in Appendix A. The 0° - 15° cross-polarized measurements were removed from the plot because of the limited polarization purity of the antennas. The leakage here from the strong co-polarized backscatter measurements affects the cross-polarized measurements even with vector correction. The absolute

calibration was done with a metal sphere.

5. Results

Figure 1 shows the radar power return as a function of range for the radar for VV pol. at 0°. This spectrum shows a strong return at about 2m, which corresponds to the ice sheet. The SNR is > 40dB. Figure 2 summarizes the experiment by showing σ° at 0° throughout the course of the experiment. The backscatter vs. thickness is shown in Figure 3 at three incidence angles. The primary objective was to study roughness schemes hence we did not collect data needed to study initial growth phase.

The backscatter variation of normal incidence with and without snow cover are shown in Figure 4. Here we observe that for bare ice there is < 1 dB variation in σ° and its mean value is 16 dB. After applying a snow fall, the mean σ° dropped by about 10 dB and had considerably more variation with σ° ranging from 1 to 14 dB. This is consistent with a roughening of the surface, believed to be caused by brine-wicking into the snow layer.

Angular plots of σ° for each polarization are shown in Figures 5 - 13. Measurements are shown with vector calibration. The scalar-calibrated results are in Appendix A for comparison.

6. Summary

Measurements were taken under controlled conditions from simulated sea ice to determine the radar backscatter of different thickness and surface types of sea ice. The data were processed using both scalar and vector calibration techniques. The vector calibration technique improved the quality of cross polarized measurements considerably.

These data have been supplied to the modelers for determining backscatter mechanisms and to investigate the effect of ice growth on the backscatter signature (Zabel et al., 1994).

7. References

Beaven, S. G., 1992, "Radar Backscatter Measurements from Simulated Sea Ice and Arctic Sea Ice During the Fall Freeze-up," M.S. Thesis, University of Kansas, 1992.

Beaven, S.G., G.L. Lockhart, S.P. Gogineni, K.C. Jezek, R. Hosseinmostafa, A.J. Gow, D.K. Perovich, A.K. Fung, and S. Tjuatja, "Laboratory Measurement of Radar Backscatter from Bare and Snow-covered Saline Ice Sheets." recommended for acceptance in *International Journal of Remote Sensing*, submitted Jan. 1994.

Izuka, K., Freundorfer, A.P., Wu, K.H., Mori, H., Ogura, H., and Nguyen, V.K., "Step-frequency radar," *Journal of Applied Physics*, vol. 56, no. 9, pp. 2572-2583, 1984.

Ulaby, F.T., Moore, R.K., and Fung, A.K., *Microwave Remote Sensing: Active and Passive*, vol. III, (Norwood, MA: Artech House), 1986.

Zabel, I.H.H., Jezek, K.C., Gogineni, S.P., and Kanagaratnam,P., "Roughness and Permittivity as Proxy Indicators of Sea Ice Thickness: A Simulation," Submitted to JGR-Oceans, 1994.

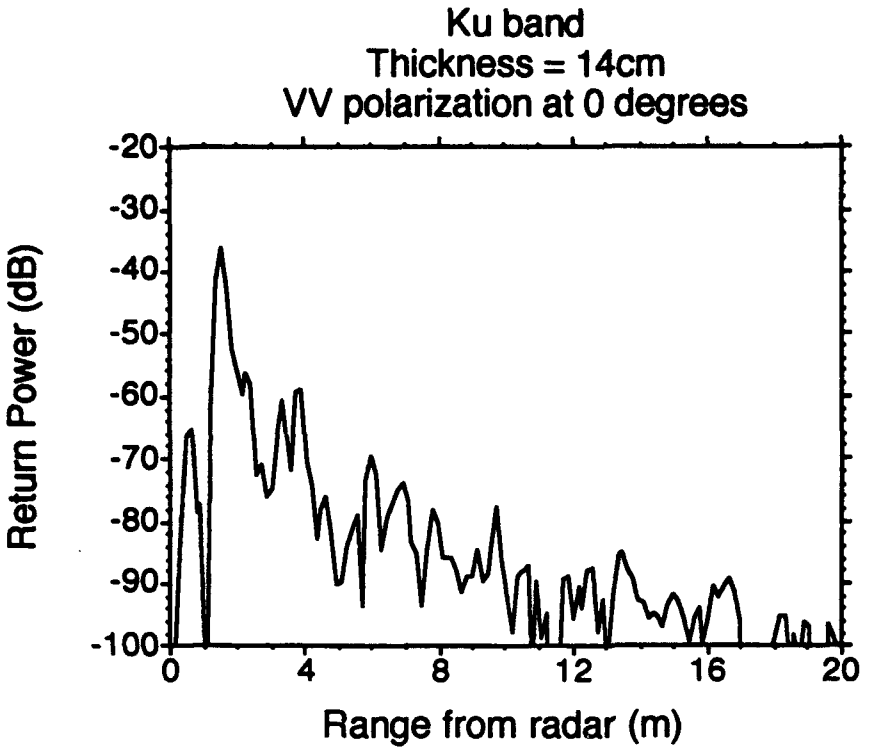

Figure 1. Plot of typical return power as a function of distance from radar for VV polarization at 0 degrees.

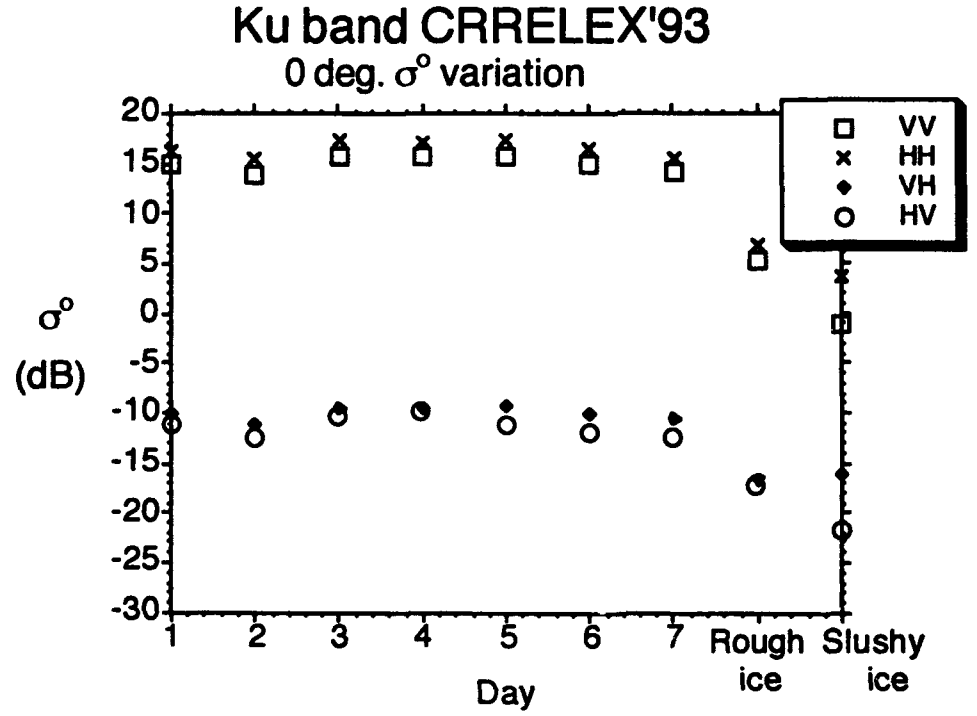

Figure 2. Plot of backscattering coefficient at 0 degrees on different days/ice types for all 4 polarizations.

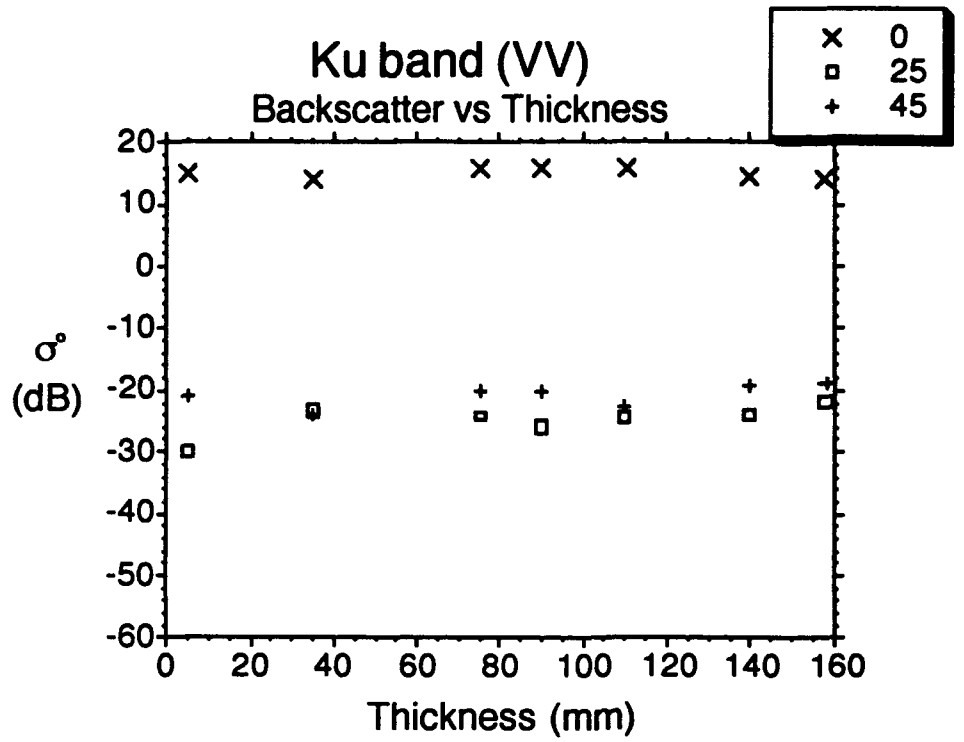

Figure 3a. Plot of backscattering coefficient (VV pol.) as a function of ice thickness at 3 angles.

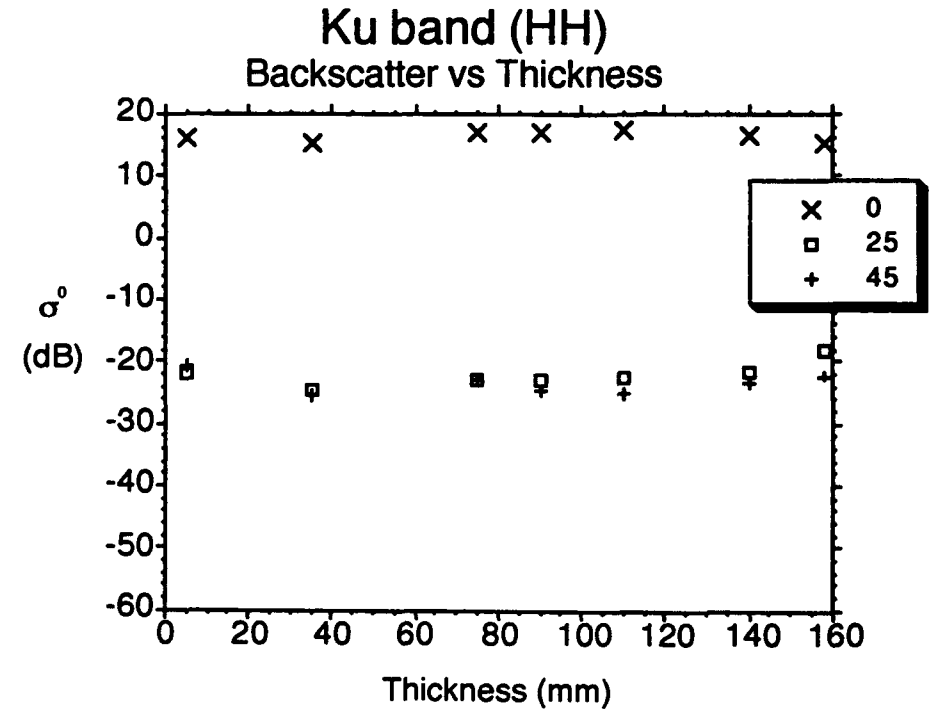

Figure 3b. Plot of backscattering coefficient (HH pol.) as a function of ice thickness at 3 angles.

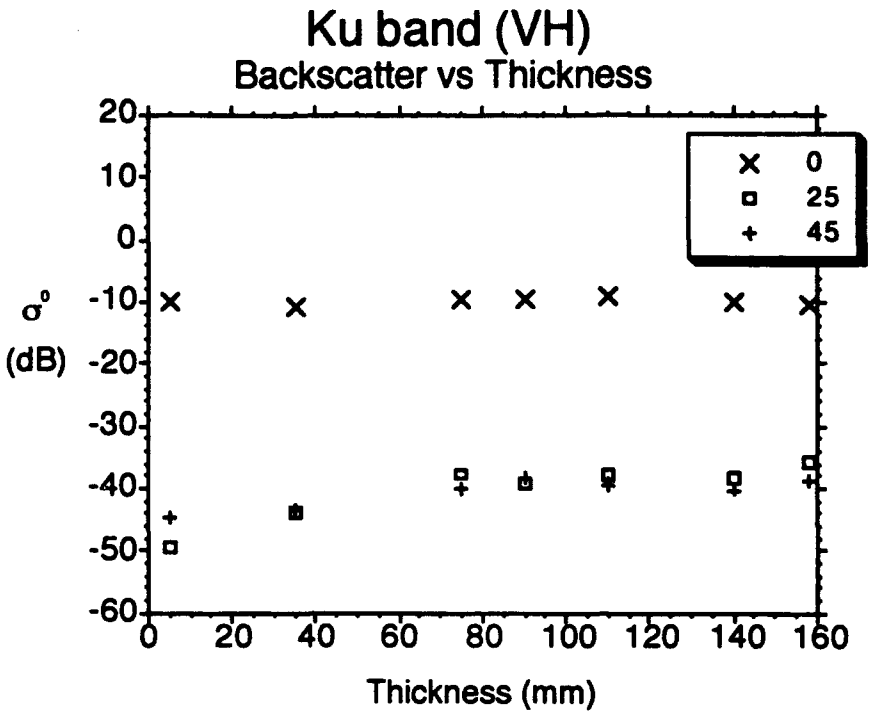

Figure 3c. Plot of backscattering coefficient (VH pol.) as a function of ice thickness at 3 angles.

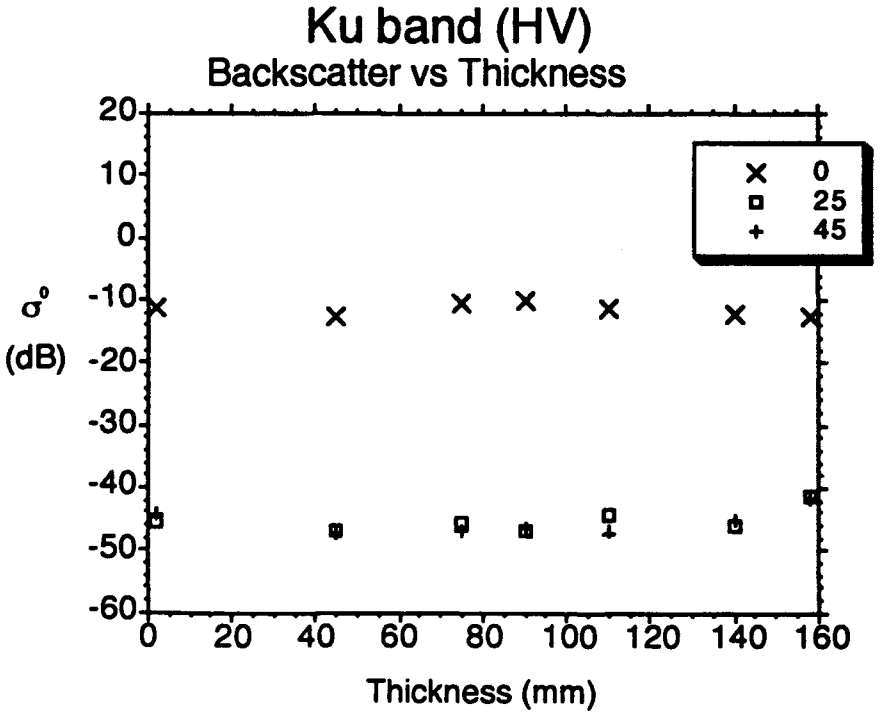

Figure 3d. Plot of backscattering coefficient (HV pol.) as a function of ice thickness at 3 angles.

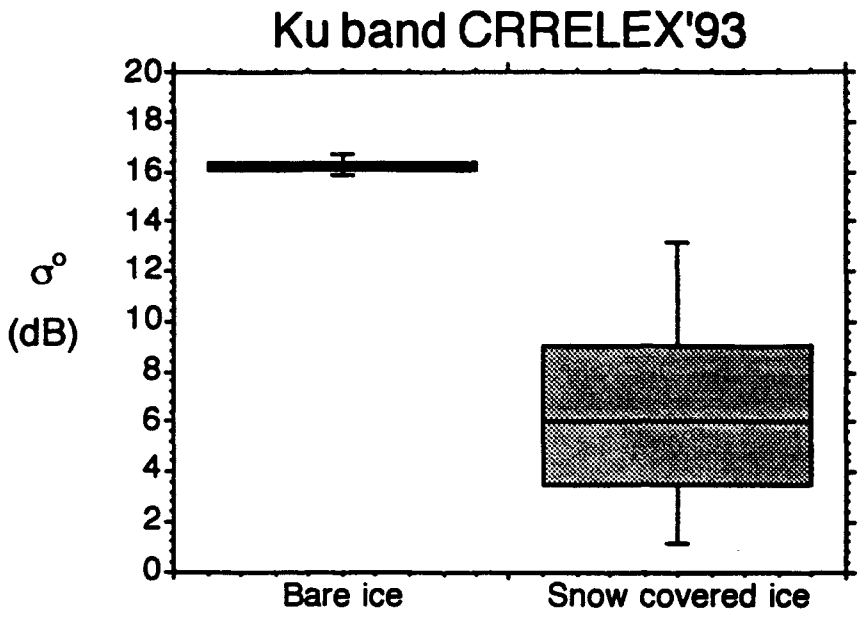

Figure 4. Plot of variation in backscattering coefficient for bare ice and snow covered ice.

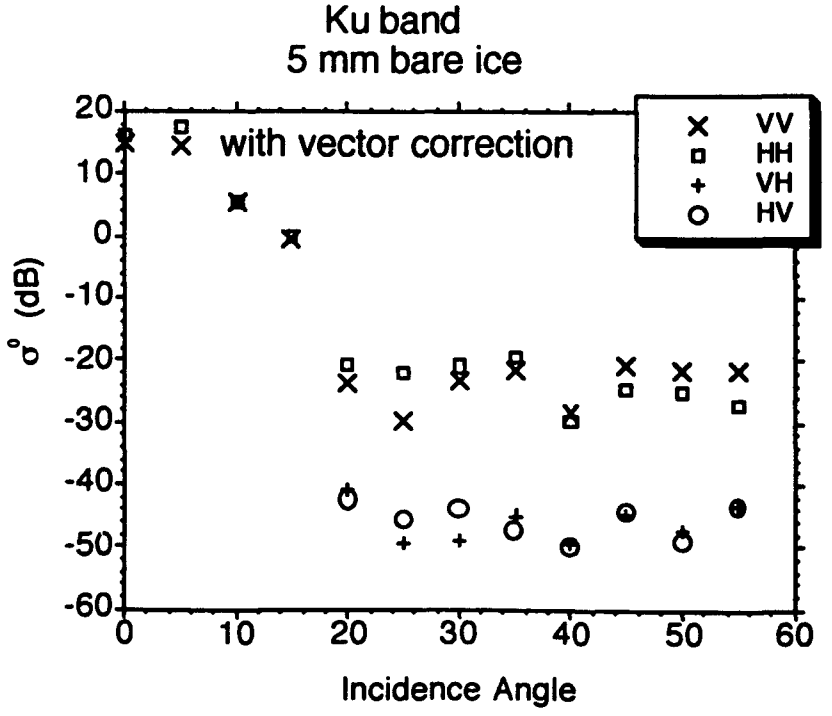

Figure 5. Plot of backscattering coefficient as a function of incidence angle for 5-mm bare ice.

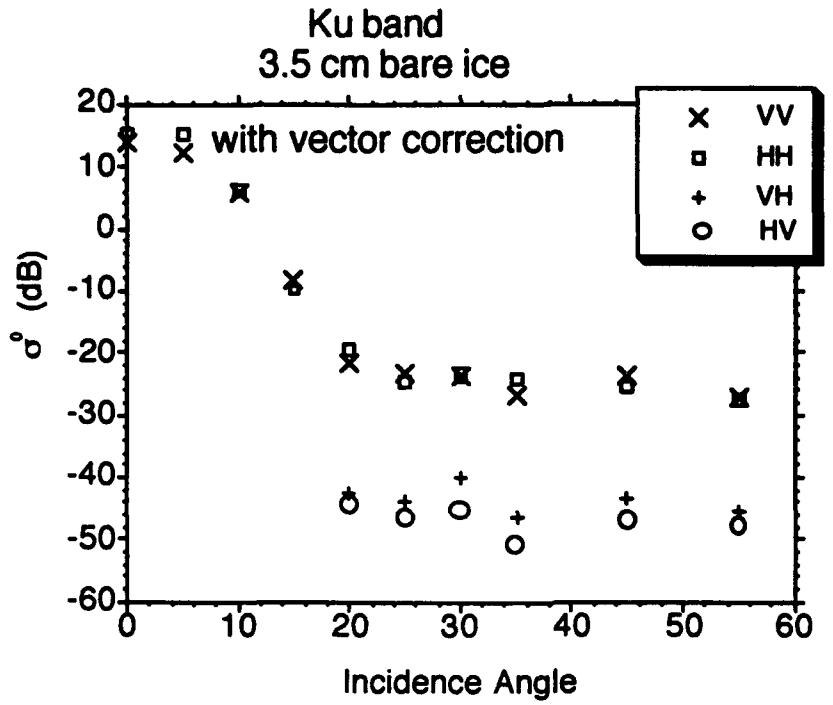

Figure 6. Plot of backscattering coefficient as a function of incidence angle for 3.5-cm bare ice.

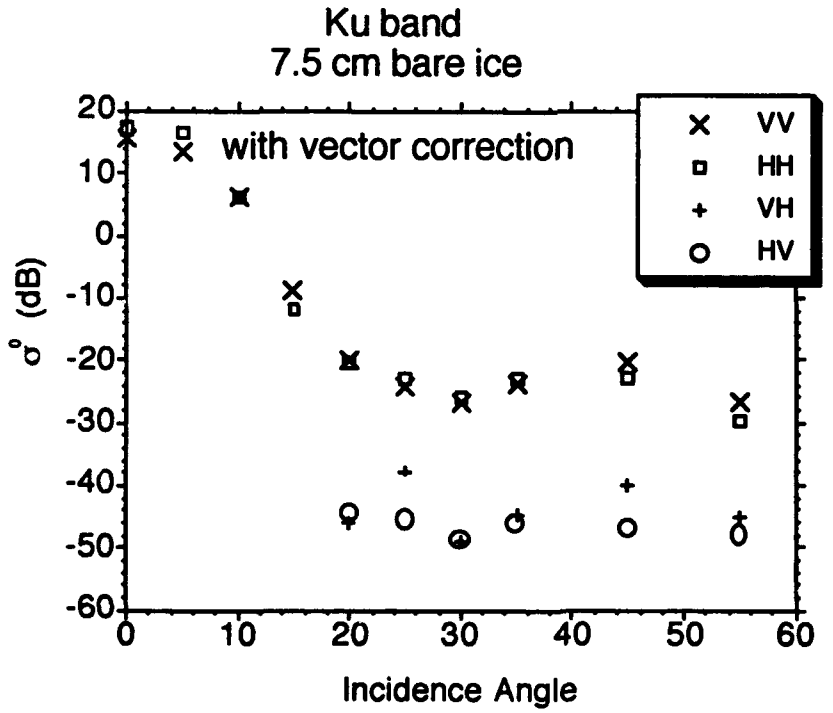

Figure 7. Plot of backscattering coefficient as a function of incidence angle for 7.5-cm bare ice.

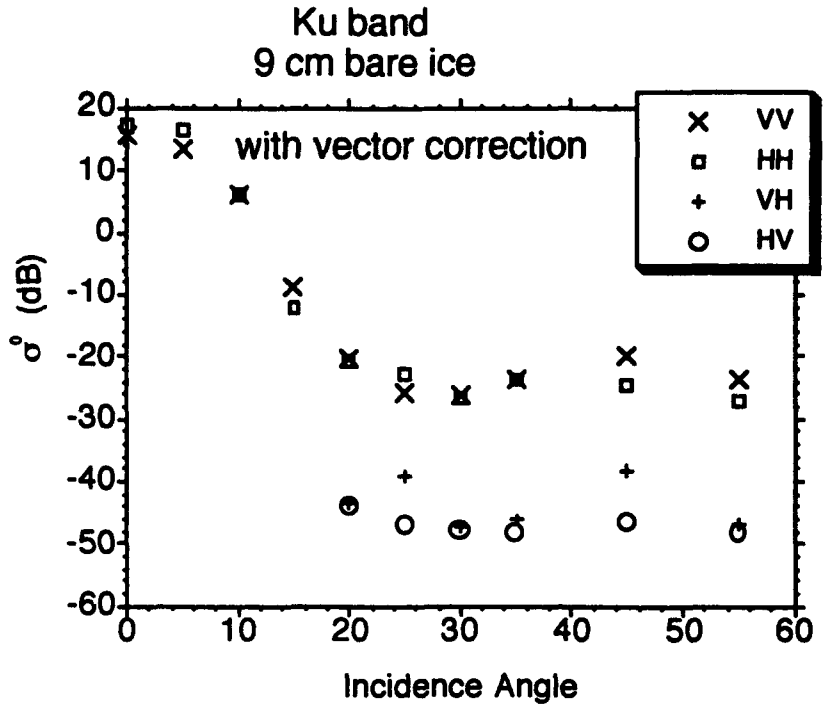

Figure 8. Plot of backscattering coefficient as a function of incidence angle for 9-cm bare ice.

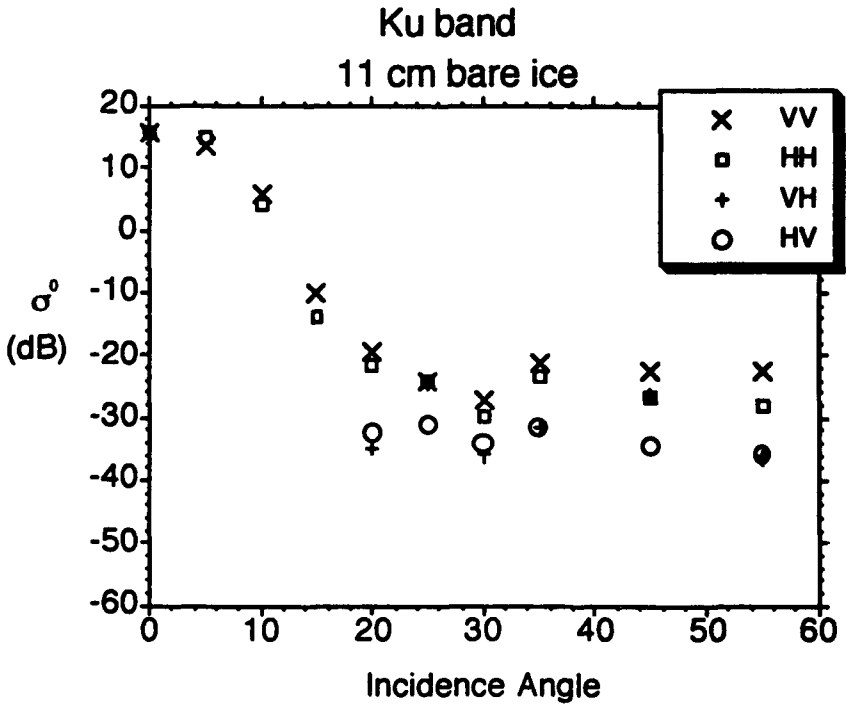

Figure 9. Plot of backscattering coefficient as a function of incidence angle for 11-cm bare ice.

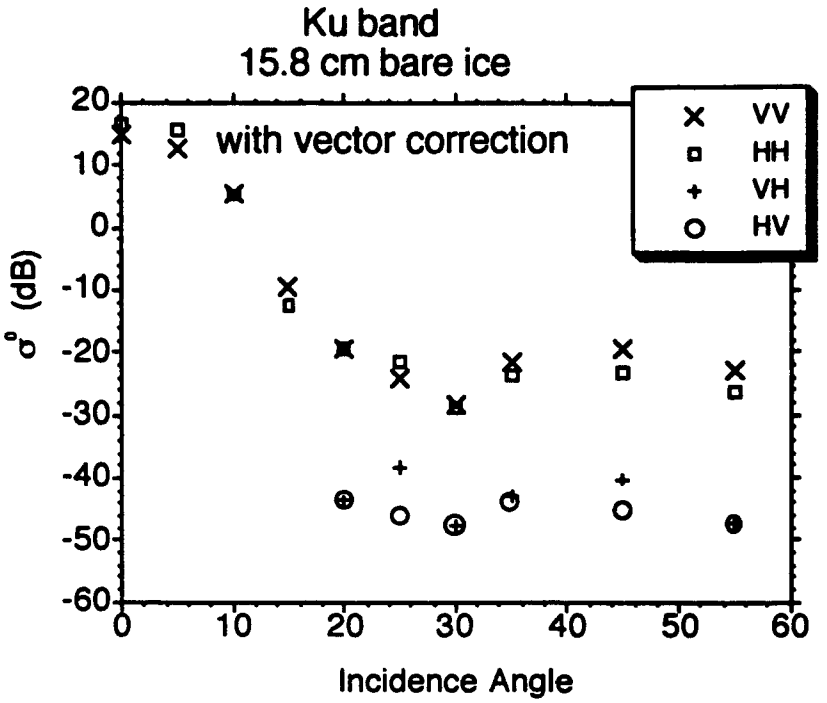

Figure 10. Plot of backscattering coefficient as a function of incidence angle for 15.8-cm bare ice.

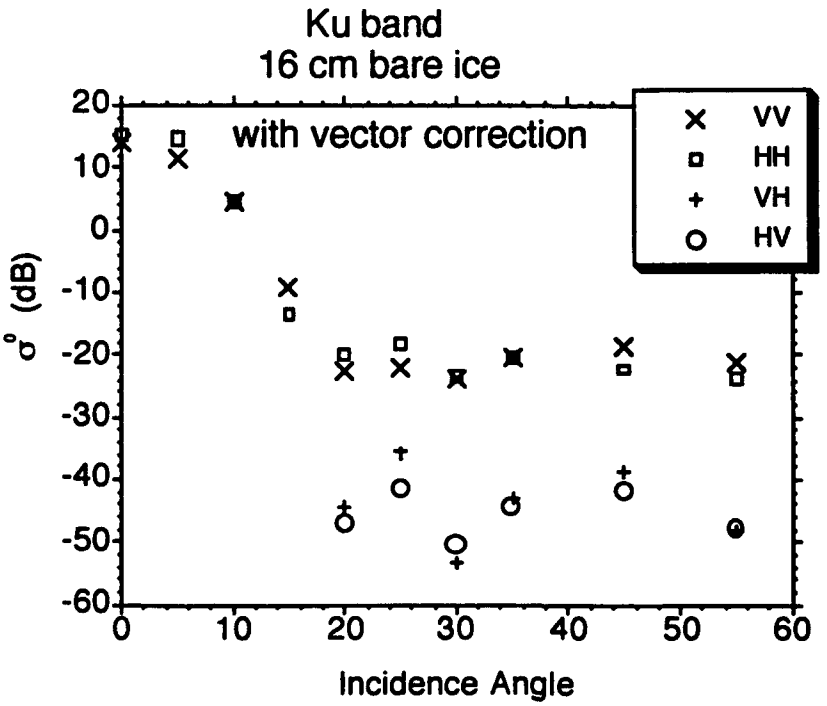

Figure 11. Plot of backscattering coefficient as a function of incidence angle for 16-cm bare ice.

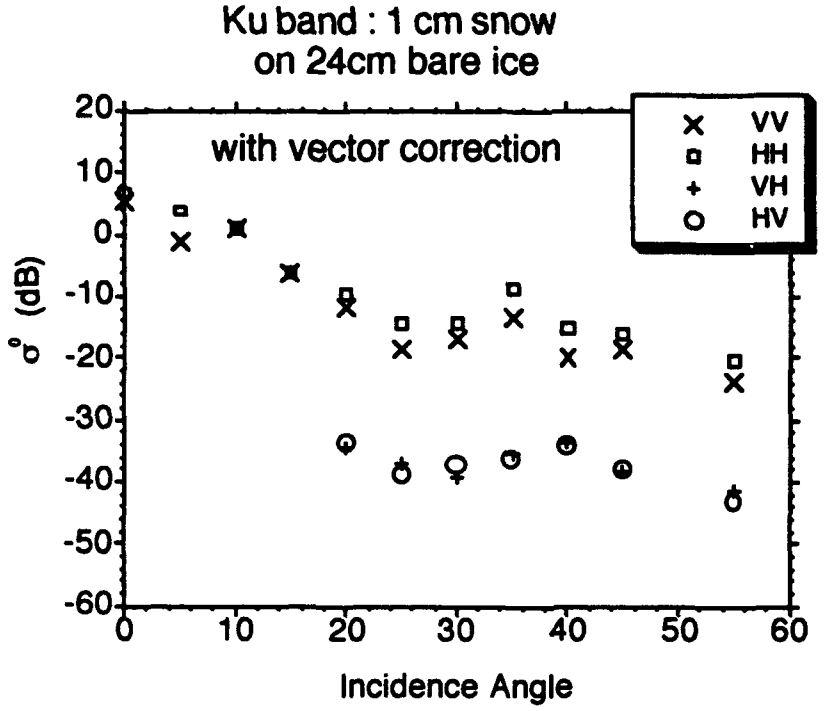

Figure 12. Plot of backscattering coefficient as a function of incidence angle for snow covered bare ice.

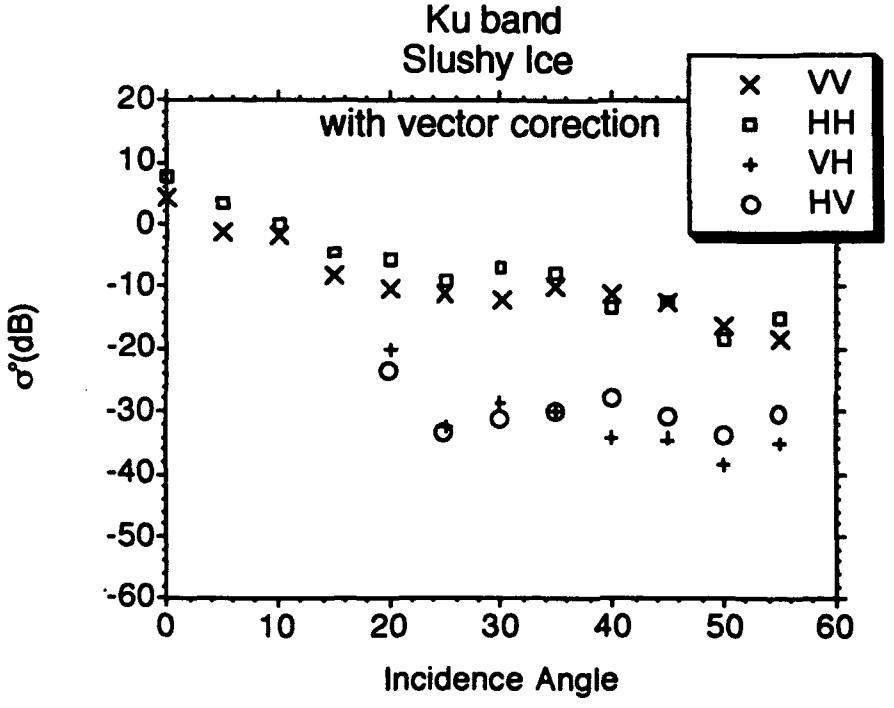

Figure 13. Plot of backscattering coefficient as a function of incidence angle for slushy ice.

APPENDIX A: Plots of Backscattering coefficients using scalar calibration

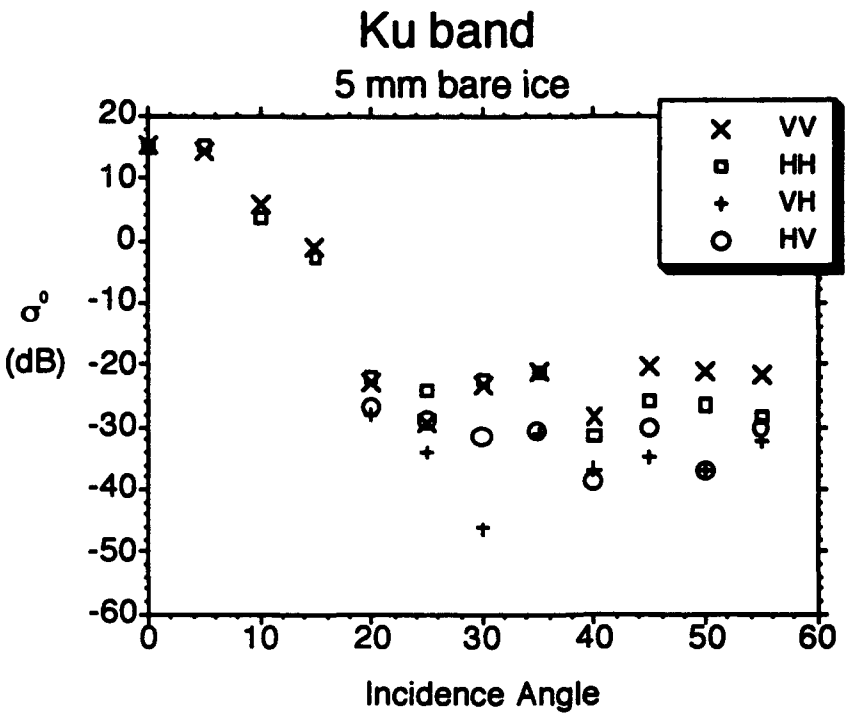
Ku band
5 mm bare ice
VV
HH
VH
HV
σ°
(dB)
20
10
0
-10
-20
-30
-40
-50
-60
0
10
20
30
40
50
60
Incidence Angle

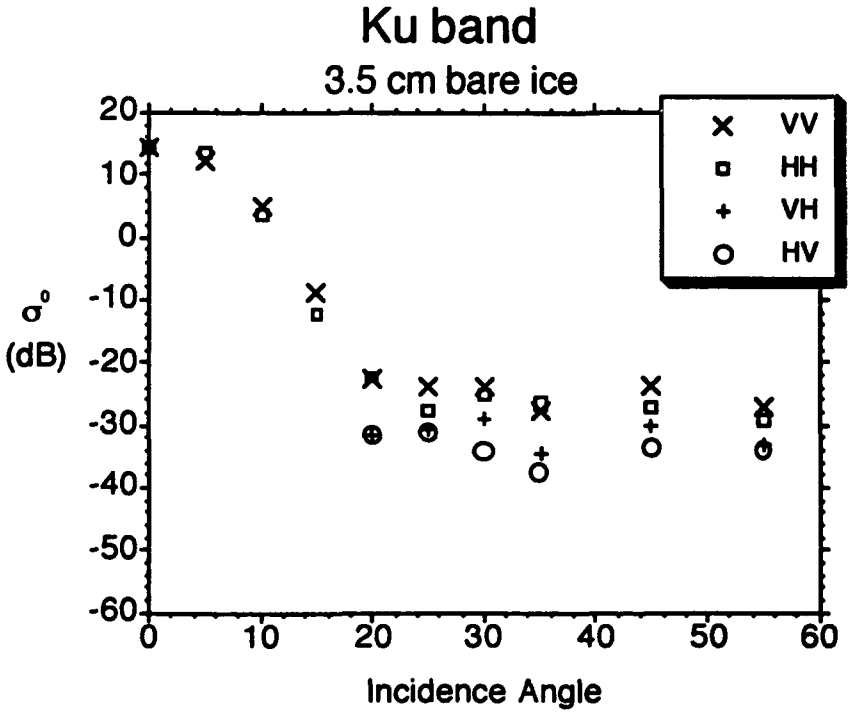
Ku band
3.5 cm bare ice
VV
HH
VH
HV
σ°
(dB)
20
10
0
-10
-20
-30
-40
-50
-60
0
10
20
30
40
50
60
Incidence Angle

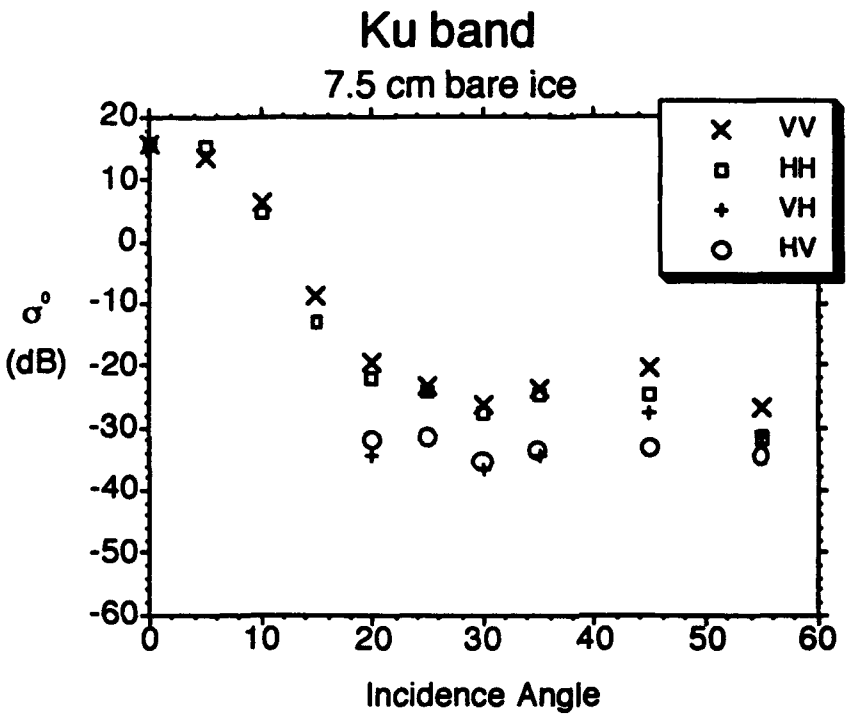
Ku band
7.5 cm bare ice
VV
HH
VH
HV
σ°
(dB)
20
10
0
-10
-20
-30
-40
-50
-60
0
10
20
30
40
50
60
Incidence Angle

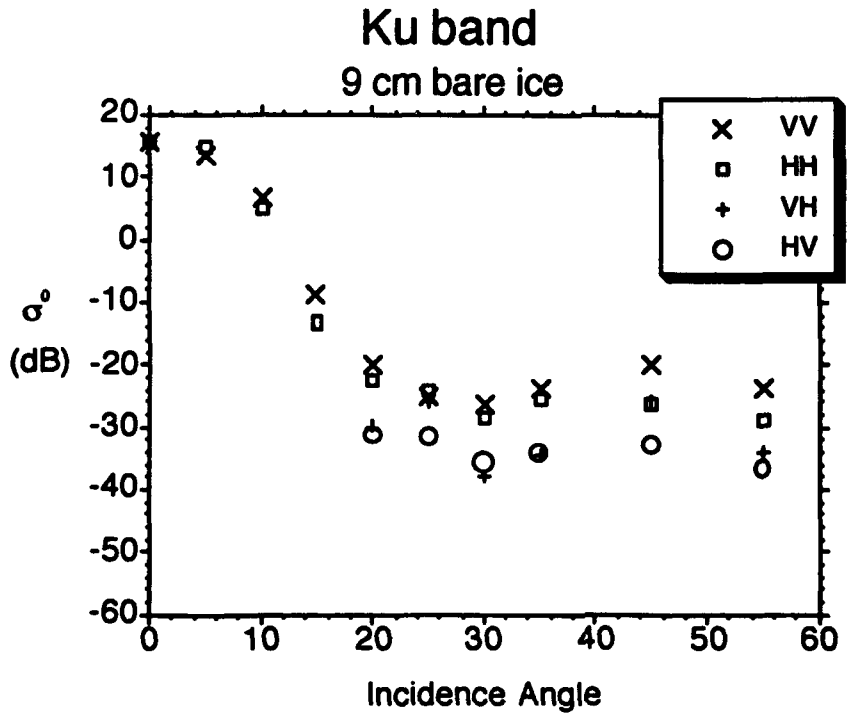
Ku band
9 cm bare ice
VV
HH
VH
HV
σ°
(dB)
20
10
0
-10
-20
-30
-40
-50
-60
0
10
20
30
40
50
60
Incidence Angle

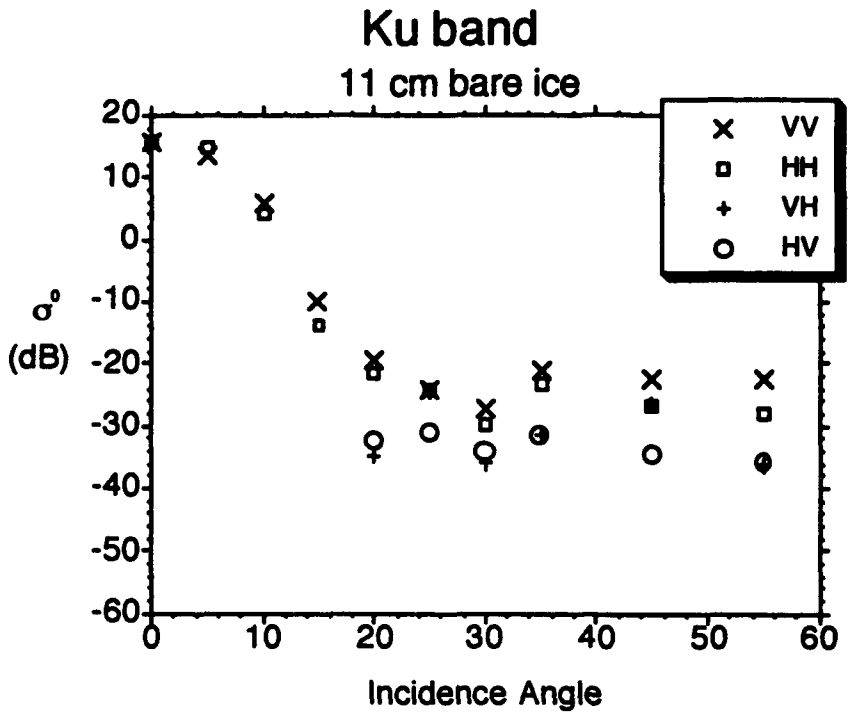
Ku band
11 cm bare ice
VV
HH
VH
HV
σ°
(dB)
20
10
0
-10
-20
-30
-40
-50
-60
0
10
20
30
40
50
60
Incidence Angle

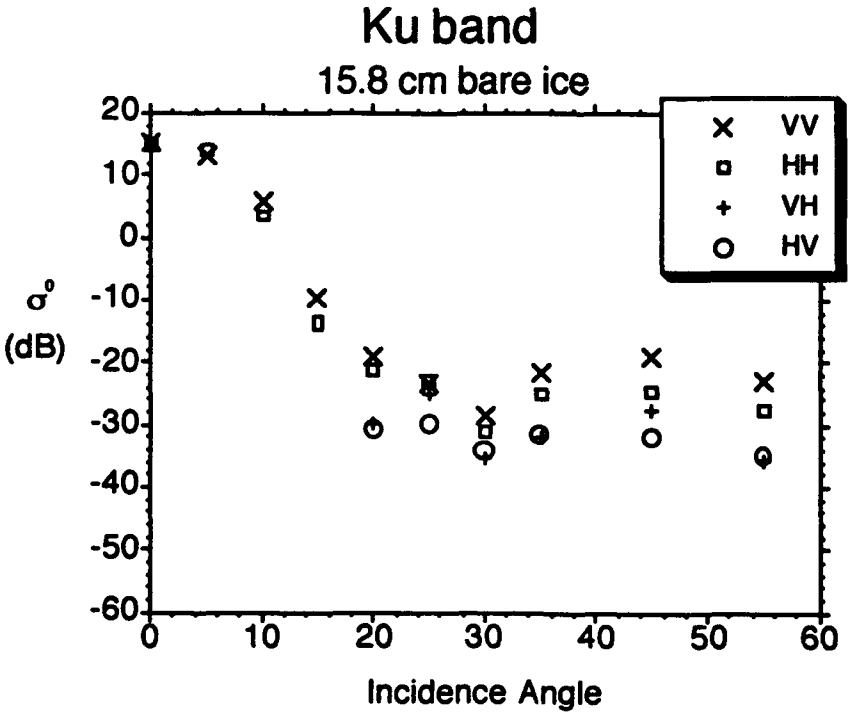
Ku band
15.8 cm bare ice
VV
HH
VH
HV
σ°
(dB)
20
10
0
-10
-20
-30
-40
-50
-60
0
10
20
30
40
50
60
Incidence Angle

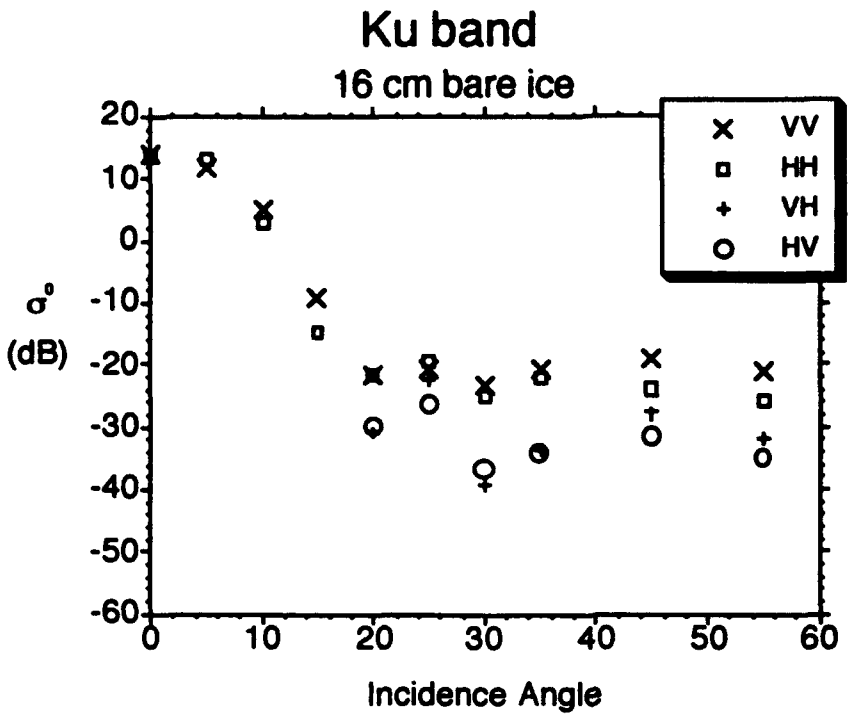
Ku band
16 cm bare ice
VV
HH
VH
HV
σ°
(dB)
20
10
0
-10
-20
-30
-40
-50
-60
0
10
20
30
40
50
60
Incidence Angle

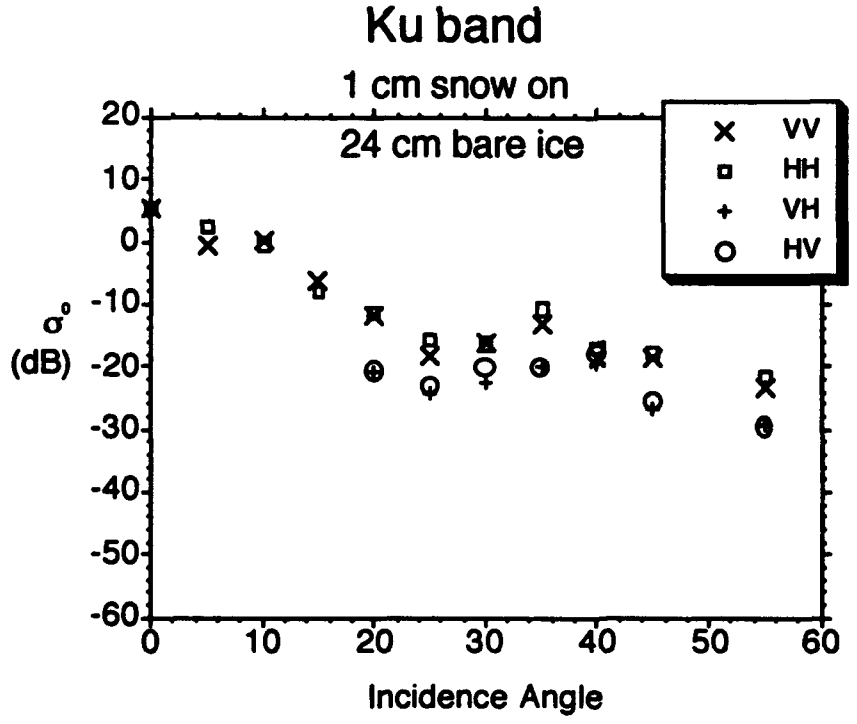
Ku band
1 cm snow on
24 cm bare ice
VV
HH
VH
HV
σ°
(dB)
20
10
0
-10
-20
-30
-40
-50
-60
0
10
20
30
40
50
60
Incidence Angle

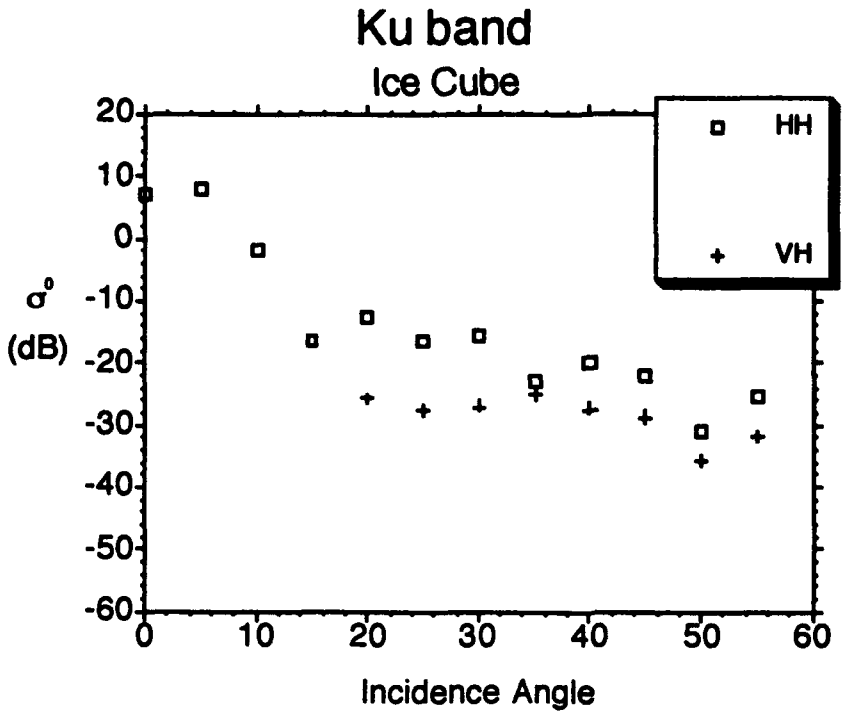
Ku band
Ice Cube
HH
VH
σ°
(dB)
20
10
0
-10
-20
-30
-40
-50
-60
0
10
20
30
40
50
60
Incidence Angle

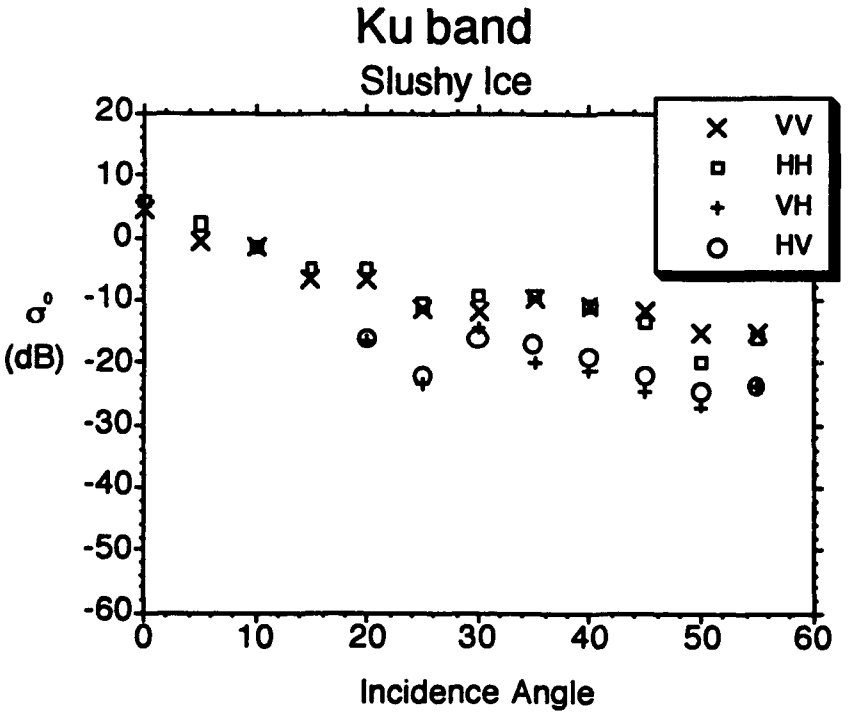
Ku band
Slushy Ice
VV
HH
VH
HV
σ°
(dB)
20
10
0
-10
-20
-30
-40
-50
-60
0
10
20
30
40
50
60
Incidence Angle